Small

NANO · MICRO small
www.small-journal.com

RESEARCH ARTICLE OPEN ACCESS

The Molecular Basis of Growth Control in Guanine Crystals

Dolev Brenman-Begin[1] | Jonathan R. Church[2,3] | Siddharth Sahoo[1] | Zohar Eyal[1] | Idan Biran[4,7] | Nir Kampf[3] | Yuval Barzilay[1] | Anna Kossoy[3] | Lothar Houben[3] | Liel Sapir[5] | Barak Hirshberg[2,6] | Dvir Gur[1]

[1]Department of Molecular Genetics, Weizmann Institute of Science, Rehovot, Israel | [2]School of Chemistry, Tel Aviv University, Tel Aviv, Israel | [3]Department of Chemical Research Support, Weizmann Institute of Science, Rehovot, Israel | [4]Department of Molecular Chemistry and Materials Science, Weizmann Institute of Science, Rehovot, Israel | [5]Department of Chemistry and the Institute of Nanotechnology and Advanced Materials, Bar-Ilan University, Ramat Gan, Israel | [6]Department of Molecular Chemistry and Materials Science Weizmann Institute of Science, Tel Aviv University, Tel Aviv, Israel | [7]Center for Visualizing Catalytic Processes (VISION), Department of Physics, Technical University of Denmark, Lyngby, Denmark

Correspondence: Dvir Gur (Dvir.gur@weizmann.ac.il)

Received: 20 August 2025 | **Revised:** 11 December 2025 | **Accepted:** 22 December 2025

Keywords: crystal growth | guanine | molecular mechanism | morphology

ABSTRACT

Precise control over crystal morphology is a longstanding challenge in materials science, as crystal shape governs optical, mechanical, and electronic properties. In contrast, living organisms achieve remarkable control over crystal morphology, though the underlying mechanisms are not fully understood. Among the most common organic materials are guanine crystals, notable for their plate-like morphology and high anisotropic refractive index, arising from the stacking of hydrogen-bonded molecular layers along the (100) plane. Here we show that simple synthetic polymers not only reproduce this biogenic plate-like form in vitro but also expand the accessible morphology space to prisms and needles by systematically varying i) multivalent interactions, ii) functional-group identity, and iii) polarity and hydrogen-bonding capacity. Using microscopy, spectroscopy, and molecular dynamics simulations, we find that carbonyl-bearing polymers selectively adsorb to the (100) stacking face, cap layer addition along the *a*-axis, and yield large plates indistinguishable from biogenic crystals. In contrast, reducing carbonyl polarity, increasing steric-bulk, or introducing highly-polar groups redirect adsorption and produces bulkier prisms or slender needles. Simulations corroborate facet selectivity, identify contact motifs involving carbonyl oxygens and adjacent methylenes. Together, these findings provide design principles for sculpting organic crystals and suggest analogous interactions exploited by biological scaffolds to orchestrate guanine assembly.

1 | Introduction

Controlling the 3D morphology of crystals is a longstanding challenge in materials science, with profound implications for optimizing optical, mechanical, and electronic properties [1–8]. While synthetic crystallization methods often struggle to precisely dictate crystal shape and growth direction, biological systems routinely produce crystals with highly specific morphologies tailored to their function (Figure 1) [9–22]. A striking example is the formation of biogenic guanine crystals in animals, which adopt a thin plate-like morphology (Figure 1E–G) that deviates from the thermodynamically favored prism shape (Figure 1A,B; Figures S1A–C and S2A) [9, 10, 23–26]. This morphology is not only unusual but also functionally crucial: guanine platelets possess an extremely high in-plane refractive index (~1.83) [9, 10, 27–29], rivalling many inorganic crystals and enabling exceptional optical effects such as structural coloration and broadband reflectance [10, 11]. In copepods [30, 31], scallops [32, 33], zebrafish [34], and many other organisms, stacks or arrays of plate-like anhydrous guanine crystals serve as reflective

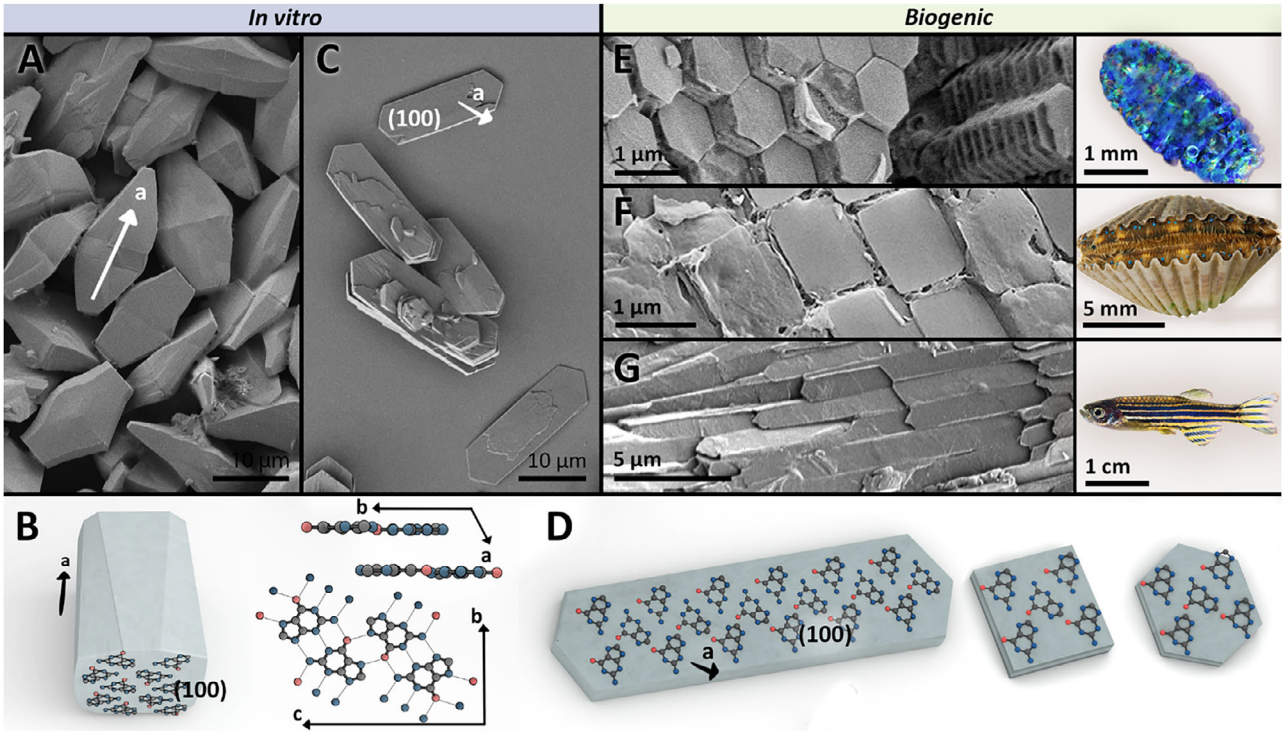

FIGURE 1 | Control over guanine crystal morphology in biogenic and synthetic systems. (A) Synthetic guanine crystal exhibiting prismatic morphology, which was grown from formamide solution. (B) Schematic illustration of a prismatic guanine crystal, characterized by rapid growth along the *a*-axis (left). Schematic illustration showing the molecular arrayment within a β-guanine crystal from different perspectives (right). Gray: Carbon, blue: Nitrogen, and red: Oxygen. (C) Synthetic guanine crystal formed in the presence of the copolymer PVP-co-VA, displaying a plate-like morphology due to suppressed growth along the *a*-direction, which was grown from formamide solution. (D) Schematic of a plate-like guanine crystal, with inhibited growth along the *a*-axis. Gray: Carbon, blue: Nitrogen, and red: Oxygen. (E–G) Cryo-SEM images of naturally occurring, plate-like guanine crystals: from the argentum of the copepod Sapphirina metallina (E), the eye of the scallop Argopecten irradians (F), and the iris of the zebrafish Danio rerio (G). Cryo-SEM images of the copepod *Sapphirina metallina* (E), scallop Argopecten irradians (F) and zebrafish Danio rerio (G) were adopted with permission from JACS [31], Science [33] and Advanced Materials [35] journals respectively. Photo credit of scallop organism image (F, right image): David Liittschwager.

mirrors or photonic crystals in specialized tissue (Figure 1D–G). The optical excellence of guanine is thus closely linked to its morphology [35], making it imperative to understand and control the factors that direct guanine crystal growth into these unique forms.

Guanine crystallizes in two main anhydrous polymorphs, both built from 2D sheets of molecules hydrogen-bonded in the (100) plane, but distinguished by how those sheets stack along the *a*-axis [24, 36, 37]. In the metastable β form (space group $P112_1/b$), adjacent layers are offset along the *b*-axis, whereas in the thermodynamically favoured α polymorph (space group $P12_1/c1$), they shift along the *c*-axis [36]. Together with a third proposed form γ, in which molecular layers stack in a zigzag mode [36]. Biogenic systems overwhelmingly produce the β polymorph [35, 36, 38, 39], but in vitro growth often begins with β phase that gradually transforms into the α phase over time [24].

Extensive studies of biogenic guanine crystallization reveal that organisms employ specialized strategies to achieve and stabilize the plate-like form. Rather than following a classical one-step nucleation and growth pathway, guanine crystals in vivo form through multi-step, "nonclassical" crystallization processes [40]. Recent work shows that guanine crystallization is templated by pre-assembled biological structures. Within cells [25, 26, 41, 42], fibrillar macromolecular scaffolds (e.g., amyloid-like protein fibers or sheet-like assemblies) provide an interface for crystal nucleation and dictate the orientation of nascent crystals [25, 26]. For example, in fish [25] and mollusks [26], guanine nucleates as multiple thin crystalline leaflets on the surface of macromolecular fibers, which serve as a template aligning the crystal's basal plane parallel to the fiber [43].

Concurrently, specific biogenic molecules, likely proteins or peptides, selectively bind and cap the (100) face, thereby suppressing growth along the *a*-axis, which corresponds to the stacking direction. The net result of this biologically orchestrated process is a crystal habit dominated by a large, reflective (100) plane and a minimal dimension along the stacking direction (*a*-axis), i.e., a thin plate (Figure 1D–G). Additionally, guanine crystals are known to contain other small molecules as dopants, with hypoxanthine being the dominant one [44–46]. It was found that the percentage of hypoxanthine incorporated into the guanine crystals affects crystal morphology both in vitro and in vivo. Increasing hypoxanthine intra-crystalline levels results in more pronounced (012) facets and underdeveloped (001) facets [46, 47]. Organisms thus exquisitely control guanine crystal morphology by using a combination of small-molecule

modulators and macromolecular templates, achieving forms that maximize optical performance while circumventing the crystal's natural growth tendencies.

The exceptional optical properties of biogenic guanine crystals have inspired efforts to replicate and control their morphology synthetically [48–54]. For example, Oaki et al. and later Chen et al. showed that recrystallizing guanine on a solid support in the presence of organic modifiers or polymers like poly(vinyl pyrrolidone) (PVP) and PVP-co-vinyl acetate (PVP-co-VA) promoted thin plate crystals oriented parallel to the substrate. In contrast, crystallization without these additives yielded prismatic aggregates (Figure 1C,D; Figures S1D–F and S2B) [52, 55, 56]. These studies demonstrated that organic polymers can selectively modulate guanine crystal habit, an approach conceptually related to the systems examined in the present work.

Similarly, controlled solvent environments have been used to obtain plate-like guanine: guanine crystallized from certain organic solvents (e.g., DMSO) can form thin plates instead of prisms [10, 23, 54]. In aqueous systems that more closely mimic physiological conditions, Gur et al. showed that pH adjustments can direct both guanine polymorphism and crystal habit, highlighting how changes in solution chemistry can dramatically affect crystal shape, size, and internal structure [24].

Beyond guanine, these principles extend to other π-conjugated systems, where noncovalent contacts dictate modifier binding and facet-specific "capping". A growing body of work now recognizes three complementary interaction types: i) π–π stacking, governed by a balance of dispersion, electrostatic, and solvent effects; ii) dipole–π and cation-π contacts, in which polarized groups (e.g., carbonyls or protonated amines) engage aromatic π clouds; and iii) CH—π interactions, whose strength depends on the electropositivity of C—H donors and the electron density of the π system [57–61]. For instance, in graphene-based dispersions, polymers such as PVP or pyrene derivatives bearing electron-donating or -withdrawing substituents stabilize sheets via π–π interactions, underscoring how these weak forces can be harnessed to control the assembly and stability of planar, conjugated materials [62, 63].

Despite these advances, the molecular mechanisms by which specific modifiers, or particular functional groups, promote plate-like guanine while others do not remain poorly understood. Elucidating how modifier–guanine contacts translate into facet-selective growth inhibition is essential for building a predictive framework for crystal morphology control in guanine and other molecular systems, and for uncovering the molecular machinery underpinning biological crystallization.

In this work, we apply a reductionist approach to dissect how guanine crystal morphology is controlled at the molecular level. Inspired by the templating role of amyloid-like fibers in vivo, we use synthetic polymers as surrogate scaffolds, varying backbone length, functional-group identity, polarity, and size, to identify the key features that control crystal habit. By combining scanning electron microscopy (SEM) and low-dose cryo transmission electron microscopy (cryo-TEM) (for near-atomic comparison to biogenic crystals), in parallel to powder X-ray diffraction (PXRD) and Fourier transform infrared spectroscopy (FTIR) (to confirm polymorphic fidelity), and molecular-dynamics simulations (to reveal facet-selective adsorption), we map out how each polymer attribute influences both habit and internal structure. Beyond guiding synthetic crystal engineering, our findings also shed new light on the noncovalent interactions that likely govern guanine assembly in biological systems, offering mechanistic insight into how living cells harness dipole-π, π–π, and CH—π contacts to sculpt the ultrathin plates central to many natural photonic structures.

2 | Results

2.1 | Crystallization in the Presence of PVP-co-VA Produces Guanine Plates Indistinguishable From Biogenic Crystals

To determine whether the thin, plate-like crystals grown with PVP-co-VA are not only morphologically but also structurally equivalent to their biogenic counterparts, we performed high-resolution, low-dose cryo-TEM on both in vitro grown plates and guanine crystals extracted from zebrafish skin (Figure 2). Synthetic crystals were grown from formamide solutions following the procedure of Chen et al. (see Materials and Methods) [56]. Strikingly, the two sets of crystals were essentially indistinguishable: both exhibited the same inhibited growth along the stacking direction (a-axis), resulting in extended (100) face (Figure 2A,D), and both showed well-defined, continuous lattice fringes without any grain boundaries (Figure 2B,E). These structural similarities were further supported by Fast Fourier Transform (FFT) analysis, which revealed nearly identical patterns and spacings corresponding to the (100) plane in both crystal types (Figure 2C,F).

2.2 | The Polymer's Role in Crystal Growth

We next sought to understand which aspects of the polymer are responsible for the observed morphology control. PVP-co-VA backbone bears two distinct functional units, pyrrolidone rings (as in PVP) and acetate groups (as in PVA) (Figures 1C and 3A; Figure S1D–F). To isolate their roles, we crystallized guanine in the presence of each homopolymer under identical conditions. PVP yielded well-defined, single-crystal plates, in line with its known efficacy as a morphology modifier, and very similar to the crystals obtained with PVP-co-VA (Figure 3B; Figure S3A–C) [55, 56]. In contrast, PVA produced aggregates of ultrathin guanine leaflets, suggesting a stronger driving force for crystallization (Figure 3C; Figure S3D–F). Crystallization without any polymer gave the expected bulky prisms dominated by fast a-axis growth (Figure 1A; Figure S1A–C). In the absence of polymers, however, the morphology of individual crystals varied more between replicates, reflecting the stochastic nature of spontaneous nucleation and growth. Despite this variability, all control samples consistently exhibited a dominant tendency for elongated, prismatic growth along the a-axis. Thus, the presence of PVP or PVA causes a growth tendency toward platelet crystals.

We next examined whether the polymer chain length plays any role in its ability to modulate crystal shape. Using PVP as a

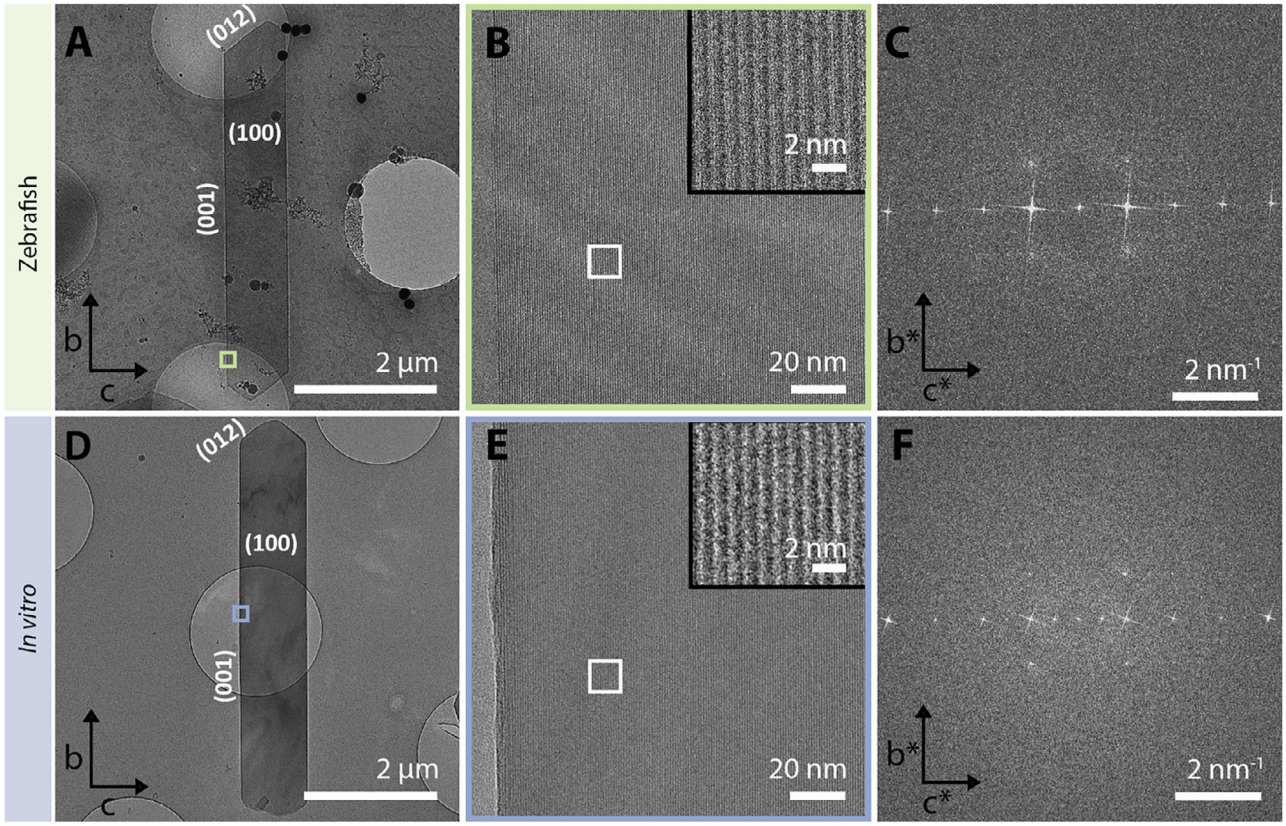

FIGURE 2 | Biogenic and synthetic plate-like crystals are structurally similar at near-atomic resolution. (A–C) Cryo-TEM images of biogenic guanine crystals isolated from the eye of an adult zebrafish. (D–F) Cryo-TEM images of synthetic guanine crystals formed with PVP-co-VA with plate-like morphology. (B,E) High-resolution cryo-TEM images showing the lattice fringes, with similar periodicity for both biogenic and synthetic crystals. Insets show a "zoom-in" view of the area highlighted by a white square. (C,F) FFT analysis shows nearly identical patterns and spacings of the guanine (100) plane of both the biogenic and synthetic crystals.

representative polymer, we compared a broad range of molecular weights from ~3.5 kDa (≈31 monomer units) up to ~1300 kDa (≈11,700 monomer units). Across this span of more than two orders of magnitude in chain length, we observed no significant difference in the crystal morphologies: all PVP samples, from shortest to longest, consistently produced thin plate-like guanine crystals (Figure S4). To further quantify this observation, we performed AFM measurements to compare crystal dimensions and aspect ratios (b/a and c/a) across the different molecular weights. While small variations were detected, no clear correlation between chain length and morphology was observed. In addition, viscosity measurements of the corresponding polymer solutions revealed only minor differences, with the lowest viscosity recorded for the highest molecular weight sample (1,300 kDa), but no consistent relationship was found between viscosity and the measured crystal aspect ratios.

These findings indicate that neither polymer chain length nor viscosity substantially influences the resulting crystal morphology. This suggests that the polymeric nature of the modifier, i.e., having multiple repeat units that can cooperatively interact with the crystal, is important, but once a threshold of polymeric character is reached, the precise chain length and entanglement are not critical factors for morphology control (at least under our conditions). Thus, the key effect arises from multivalent polymer–surface interactions rather than from viscosity or chain-length-dependent effects. Even relatively short PVP chains can act as effective crystal growth modifiers, presumably by adhering to specific crystal surfaces via their functional groups.

To further disentangle the contributions of the polymer backbone vs functional groups, we devised two complementary tests: i) using a polymer that has no functional groups at all, and ii) using the isolated functional group molecules without a polymer backbone. For the first test, polyethylene, a simple —CH_2—CH_2— chain with no polar functional groups, was added to the guanine crystallization. The result was essentially identical to the control: bulky, irregular prismatic crystals with no sign of growth inhibition along the a-axis (Figure 3D; Figure S3G–I). This indicates that a bare hydrocarbon chain, even a long one, cannot direct guanine morphology; the polymer must contain some functional moieties to interact with the crystal. For the second test, we added small-molecule analogues of the PVP-co-VA functional groups in the absence of any polymer backbone. Specifically, we tested 2-pyrrolidone, mimicking the PVP functional group, and methyl acetate, mimicking a PVA functional group, as modifiers on their own. In both cases, guanine crystallization again produced bulkier crystals similarly to the no-modifier case (Figure 3E,F; Figure S3J–O). Even when we added these small molecules together with a polyethylene backbone, simulating a "mixed" system of a bare backbone

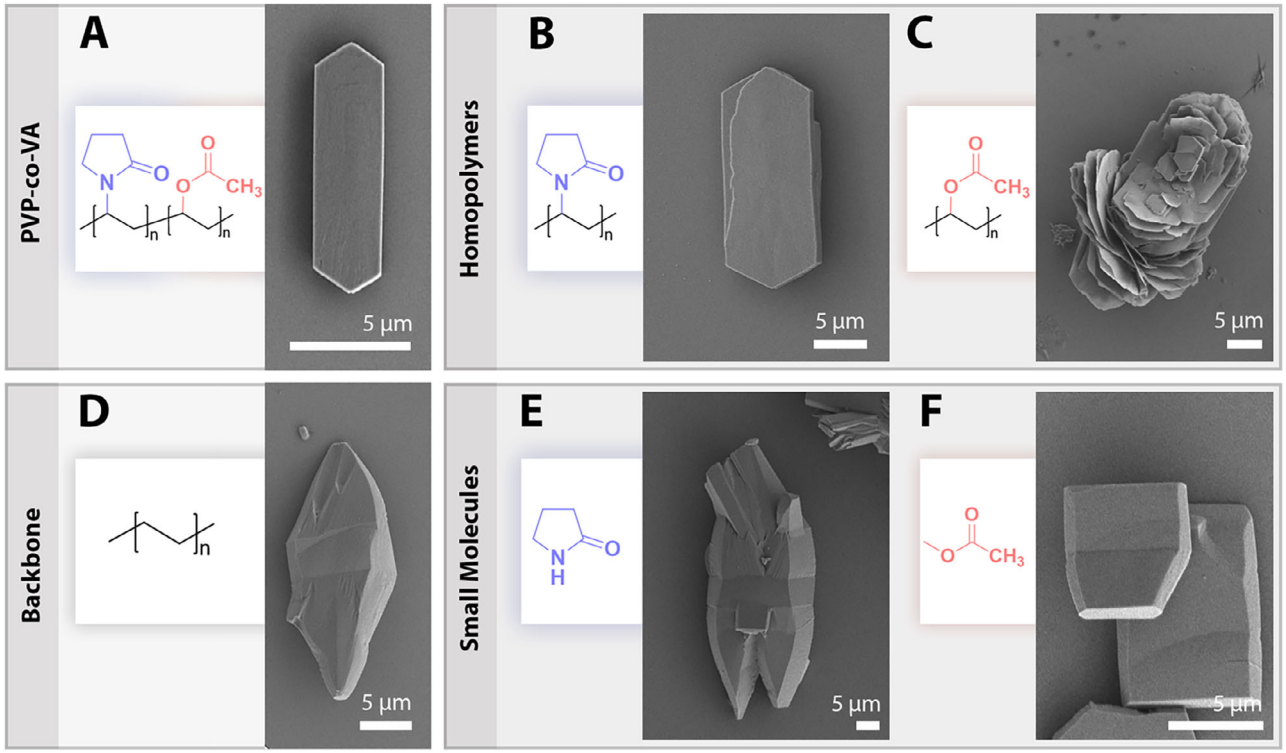

FIGURE 3 | Distinct components of the copolymer PVP-co-VA differentially influence guanine crystal morphology. A–F) SEM images of guanine crystals formed in the presence of various polymers and small molecules. Crystals formed with PVP-co-VA (A), poly(vinyl pyrrolidone) (PVP) (B), and poly(vinyl acetate) (PVA) (C), exhibit a plate-like morphology, characterized by inhibited growth along the *a*-axis. In contrast, crystals formed in the presence of polyethylene (D), 2-pyrrolidone (E), or methyl acetate (F) display a prismatic morphology, indicating a loss of directional growth inhibition.

plus free functional groups, the crystals remained thick and prism-like (Figure S5). These results demonstrate a crucial point: the synergy between the polymer's backbone and its functional groups is required to achieve selective growth inhibition. Neither the backbone alone nor the mere presence of the functional group in solution is sufficient to replicate the effect; rather, the functional groups must be integral parts of a polymer chain. We infer that the polymer backbone serves as a scaffold that positions the functional groups in a multivalent, repetitive manner along the crystal interface, whereas isolated molecules likely attach only transiently or non-specifically and cannot enforce sustained growth modulation.

2.3 | Systematic Variation of Polymer Functional Groups—Steric and Polarity

Having established that intact polymers with the appropriate functional chemistry are needed, we turned to a systematic exploration of which functional group characteristics are most effective at controlling guanine crystal shape. We hypothesized that two broad factors might influence the polymer efficacy: i) the steric size of the functional group, which could affect how well the polymer can pack against the crystal surface, and ii) the polarity or specific functional group, which could affect the binding affinity to certain crystal facets.

To test steric effects, we compared a series of vinyl ester polymers of increasing alkyl chain length: poly(vinyl acetate) (—O—C(O)CH_3 side group), poly(vinyl propionate) (—O—C(O)C_2H_5 side group), and poly(vinyl butyrate) (—O—C(O)C_3H_7 side group) (Figure 4). Notably, as the alkyl chain length increased from methyl to propyl to butyl, the resulting guanine crystals became progressively thicker (Figure 4B–D; Figures S2C,D, S3D–F and S6A–F). Poly(vinyl propionate) produced plates that were thicker than those from PVA, and poly(vinyl butyrate) in turn yielded crystals thicker than those with propionate (Figure 4B–D; Figures S2C,D, S3D–F and S6A–F). In fact, with the butyrate polymer, the crystal habit began to approach a more prismatic form, indicating a substantial loss of the plate-like character (Figure 4D; Figure S6D–F). In both cases, the symmetry of the electron diffraction patterns, and the prismatic morphology of the crystals match the expected symmetry for the β-guanine phase (Figure 4C,D; Figure S2C,D). We note that in cases in which the bulk of the crystal was thick, we collected the ED from the edges of the crystals (Figure 4C,D; Figure S2C,D). In these cases, we observed a dilation in the *b*-axis, which we do not fully understand and may represent a surface distortion rather than a bulk effect.

Quantitative dimensional analysis by Atomic Force Microscopy (AFM) confirmed this trend: the average ratio of the dimensions of the crystals measured in the directions along the *b* and *c* compared to *a* (i.e., the ratios of *b/a* and *c/a* crystal dimensions) decreased as the ester side-chain length increased (Figure 4I). In essence, larger functional groups lead to less growth inhibition along the stacking direction (*a*-axis), attributed to steric hindrance, preventing the polymer from closely interacting with the crystal's (100) surface. Shorter side chains like acetate can

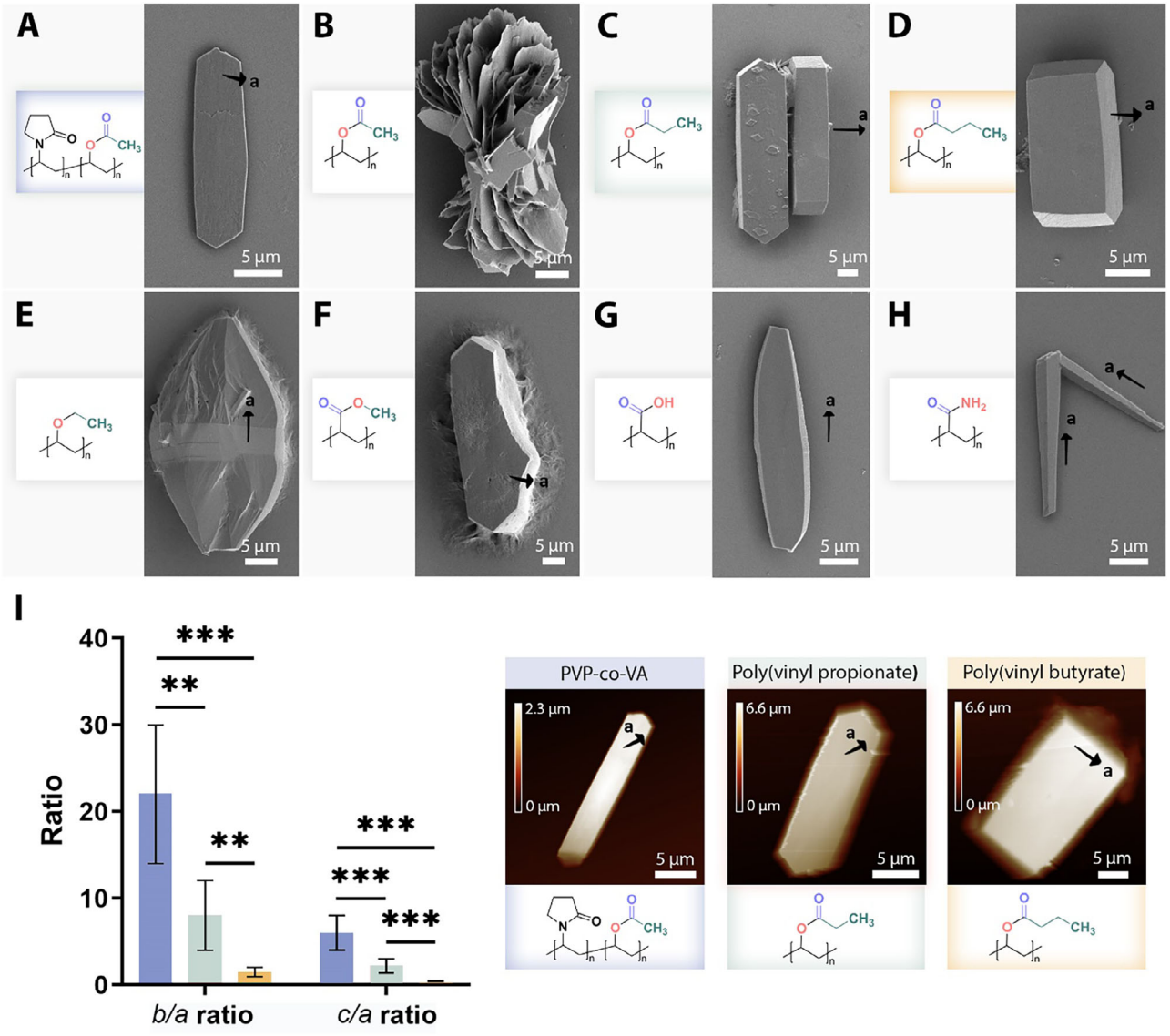

FIGURE 4 | Functional group identity modulates guanine crystal morphology. A–H) SEM images of guanine crystals formed in the presence of polymers with varying functional groups: PVP-co-VA (A), poly(vinyl acetate) (PVA) (B), poly(vinyl propionate) (C), poly(vinyl butyrate) (D), poly(ethyl vinyl ether) (E), poly(methyl acrylate) (F), poly(acrylic acid) (G), and poly(acrylamide) (H). Distinct morphologies are observed depending on the nature of the polymer's functional groups. **I)** AFM cross-section height analysis (left) and representative height images (right) of guanine crystals formed in the presence of PVP-co-VA (blue, n = 8), poly(vinyl propionate) (green, n = 6), and poly(vinyl butyrate) (yellow, n = 7). Bar graphs show the ratio of the dimensions of the crystals measured in the directions along the *a, b*, and *c* axes (*b*/*a* and *c*/*a*), quantifying the extent of growth inhibition along the *a*-axis for each condition. In which higher *b*/*a* and *c*/*a* ratios, imply stronger growth inhibition along the *a* direction. Mean values ± standard deviation are shown. Statistical significance was assessed using Welch's *t*-tests (two-tailed, unequal variances). False Discovery Rate (FDR) correction was applied for multiple comparisons. Asterisks indicate significance levels: $p < 0.05$ (*), $p < 0.01$ (**), $p < 0.001$ (***).

pack in more tightly or in greater number on the crystal surface, effectively impeding the addition of new guanine layers; by contrast, a bulky butyrate group may reduce the packing density or affinity of the polymer on that surface, and thus yielding a thicker crystal.

We next examined the role of the functional group's polarity and specific interactions. Both PVP and PVA contain a carbonyl group (C═O) in their side chains, in the lactam ring, and the ester linkage, respectively. A carbonyl can engage in dipolar interactions and has a partial negative charge on oxygen and a partial positive charge on carbon. In the guanine crystal, the (100) plane presents a flat, conjugated surface rich in π-electron density [64, 65], whereas the perpendicular planes present an array of N—H and C═O groups (hydrogen-bond donors and acceptors, Figure 1B, right) [36]. We posited that a polar functional group like a carbonyl might preferentially interact with the π-electrons-rich face of the (100) plane in an analogous manner to the dipole-π interactions [57, 66, 67], and thereby disrupt or slow further stacking in the *a* direction. To test the importance of the carbonyl itself, we tested poly(ethyl vinyl ether), a polymer that is very similar to PVA in backbone structure but has no carbonyl (its side group is —O—CH_2CH_3, an ether instead of an ester). The result was striking: guanine crystals grown with

poly(ethyl vinyl ether) were bulky and elongated along the *a*-axis, almost indistinguishable from the control crystals (Figure 4B, E; Figures S2E, S3D–F and S6G–I). The inhibition of stacking seen with PVA was entirely lost when the C—O was removed. This confirms that the carbonyl group is a critical motif for interfering with guanine's stacking direction.

Having established the necessity of a carbonyl, we next examined how its electronic environment affects the interactions of the guanine crystal and subsequently with crystal morphology. We compared poly(vinyl acetate), in which the ester carbonyl is sandwiched between an alkoxy oxygen (to the polymer backbone) and a methyl group, with poly(methyl acrylate), where the carbonyl instead lies between the polymer backbone and a methoxy substituent. This difference in structural arrangement potentially reduces the carbonyl dipole in poly(methyl acrylate) compared to PVA, and limits its accessibility due to steric effects [68]. Consistent with this, guanine crystallized with poly(methyl acrylate) produced noticeably thicker plates than with PVA (Figure 4B,F; Figures S2F, S3D–F and S6J–L), yielding a more blocky habit. This suggests that reducing the carbonyl's polarity or sterically hindering its availability weakens its selective binding to the (100) stacking face, thereby diminishing growth inhibition along the stacking direction.

We extended this idea by testing polymers with even more polar and electron-donating groups adjacent to the carbonyl: poly(acrylic acid) (—C(O)OH substituent) and poly(acrylamide) (—C(O)NH_2 substituent), both also capable of strong hydrogen bonding. In both cases, the characteristic large plate-like (100) face almost disappeared and growth re-oriented along the *a*-axis (Figure 4G,H; Figures S2G,H, S6M–R and S7). With poly(acrylic acid), guanine crystallized into elongated prisms extending predominantly in the stacking direction (Figure 4G; Figures S6M–O and S7A,B). In the presence of poly(acrylamide), this effect was even more pronounced: crystals grew as long, slender needles aligned along the *a*-axis (Figure 4H; Figures S6P–R and S7C,D). These results suggest that when the C═O dipole is reduced and the hydrogen-bonding capacity increases, the polymer no longer targets the (100) stacking face specifically. Instead, it likely binds to hydrophilic crystal edges, competing with the crystal's native hydrogen bonding, and thus resulting in a needle-like morphology which was not previously obtained for anhydrous guanine crystals.

Finally, to rule out solution effects, we evaluated both pH and polymer concentration. We measured the final solution pH for five representative polymers, PVP, PVA, PVP-co-VA, poly(acrylamide), and poly(acrylic acid), spanning the full range of morphologies. Only minor, statistically insignificant variations were observed across polymers and repeats, indicating that pH differences are unlikely to account for the changes in crystal shape (Figure S7E). The slightly lower pH observed for PVA, poly(acrylamide), and poly(acrylic acid), could explain their tendency to form aggregates due to a moderately higher driving force for crystallization. In addition, to control the concentration, we repeated all experiments at a fixed polymer concentration of 1 mM. The resulting morphologies were consistent with those obtained under our original conditions, confirming that the observed effects arise from polymer chemistry rather than concentration (Figure S8).

2.4 | Crystal Structure and Phase Analysis

Throughout these experiments, we probed whether the various polymers induced any changes in the crystalline phase or internal structure of guanine or merely altered the morphology. All crystals obtained, whether plate-like or prismatic, were confirmed by powder X-ray (PXRD) to be a mixture of α- and β-anhydrous guanine (Figure S9A). The α and β polymorphs differ primarily in the stacking offset between molecular layers, while their in-plane hydrogen-bonding networks are nearly identical; therefore, the phase composition is not expected to significantly influence the overall crystal habit [36, 47]. Fourier Transform Infrared Spectroscopy (FTIR) likewise showed the same characteristic guanine vibrational bands in all samples, indicating that the intramolecular bonding and tautomeric form of guanine remained consistent (Figure S9B). Thus, the polymers influence the kinetics of crystal growth, but not what crystallographic structure they adopt, suggesting a surface-selective interaction rather than incorporation into the lattice or templating of a new polymorph. Subtle differences were observed in the preferred orientation of the crystallites in PXRD: for plate-like crystals, the diffraction peak corresponding to the (100) plane was notably enhanced relative to the (012) peak, whereas in bulkier crystals the two peaks had a more conventional intensity ratio. In fact, the (100) / (012) peak intensity ratio was > 3.5 for the thinnest plate-like samples, vs < 2.5 for prismatic samples. This is consistent with thin plates tending to lie flat on the sample holder, thus, the flat (100) face is preferentially oriented, amplifying the (100) reflection from those stacked layers. Aside from this orientation effect, we did not find evidence of any new crystalline order or major lattice distortion due to the polymers.

2.5 | Molecular Dynamics Simulations of Polymer–Crystal Interactions

To complement our experimental findings, we performed molecular dynamics (MD) simulations to probe how polymer oligomers adsorb onto distinct guanine crystal facets. Our simulations were performed with GROMACS 2019.6 using the CHARMM36 force field [69–72]. We constructed β-guanine slabs ($38 \times 14 \times 6$ unit cells, 12,768 molecules) exposing either the (100) face (perpendicular to the stacking direction) or (001) face (perpendicular to the hydrogen bonding direction), each immersed in a 170 Å slab of formamide in the presence of $(PVP)_{31}$ (subscript denotes the number of monomers in the chain) (Figure 5A; see Material and Methods and Supporting Information sections).

Using umbrella sampling with the distance between the polymer's center of mass (COM) and the guanine slab's COM as the reaction coordinate, we computed the effective interaction free energy (potential of mean force) for PVP with each facet. The (100) face showed a pronounced free-energy minimum of ~4 $kJ{\cdot}mol^{-1}$ at ~20 Å from the slab, whereas the (001) face displayed only a shallow ~2 $kJ{\cdot}mol^{-1}$ well at ~40 Å (Figure 5B). These results indicate a clear free energetic preference for PVP binding to the (100) face (perpendicular to the stacking direction).

To further quantify the polymer–crystal interactions, we ran three independent 1 μs unbiased MD trajectories for each facet, within a ~120 Å slab of formamide. We recorded the minimum

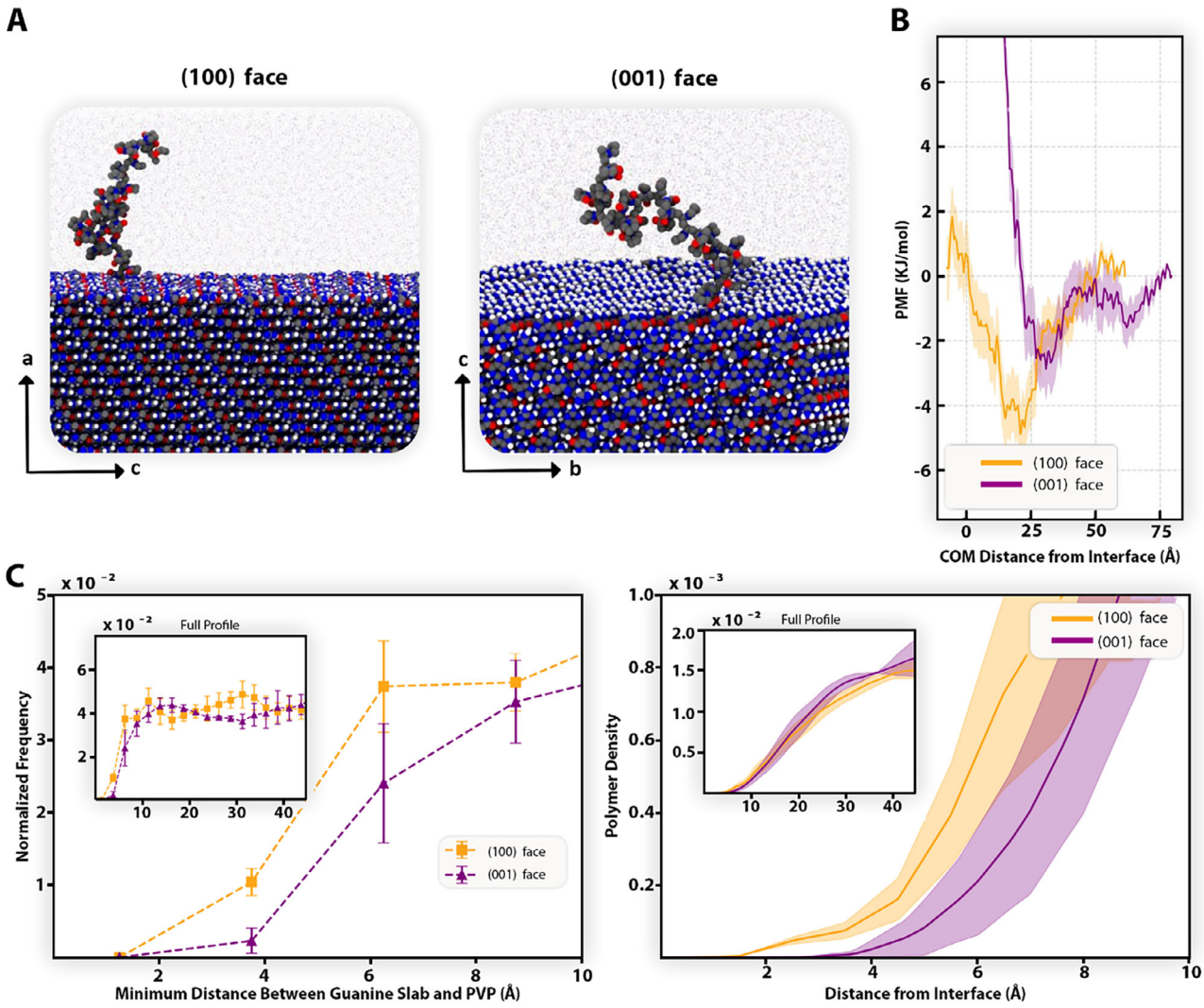

FIGURE 5 | Preferential adsorption of PVP on the guanine (100) face vs. the (001) face. (A) Snapshots of β-guanine slabs interfaced with a $(PVP)_{31}$ oligomer in formamide, viewed along the (100) face (left) and the (001) face (right). Gray: Carbon, blue: Nitrogen, and red: Oxygen. (B) Potentials of mean force for PVP approach to the (100) (orange) and (001) (purple) faces. Shaded area shows Bayesian-bootstrap errors (100 samples), highlighting the deeper free-energy minimum at the (100) face. (C) Left: Histograms of the minimum heavy-atom distance between polymer and crystal for the (100) and (001) faces, averaged over three 1 μs trajectories; error bars are standard errors. Close contacts (<5 Å) occur more frequently at the (100) face than at the (001) face. Right: Polymer heavy-atom density profiles plotted as a function of distance from the crystal interface ($z = 0$ defined by the half-maximum guanine density). The (100) face shows a pronounced increase in polymer density near the surface, indicating stronger adsorption; insets display the full histogram/density profiles into the bulk solvent.

heavy-atom distance between the polymer and the slab every 10 ps (Figures S13 and S14). On the (100) face, PVP maintained close contacts (<5 Å) in 2.07% of frames, compared to only 0.46% on the (001) face (Figure 5C, left). Corresponding polymer density profiles reinforced this facet selectivity: within 5 Å of the crystal surface, the polymer density peak was substantially higher at the (100) face than at the (001) face (Figure 5C, right).

Finally, we examined atomistic snapshots in which at least one heavy atom of a polymer residue lay within 5 Å of the slab to identify key interacting groups. Then, we quantified the number of residues that are simultaneously in close contact with the crystal surface (Figure 6A). For the (100) face, a multivalent (or multi-point) interaction is observed, consistent with the experimental results above, while for the (001) face, only a single residue is in close contact in the snapshots. In over 20% of close-contact frames at the (100) face, PVP engaged the surface via three carbon atoms plus one carbonyl oxygen; by contrast, (001) face contacts were dominated (~55%) by a single carbon atom (Figure 6B; Table S3). The second most probable contacts (Figure S16) occurred through a single carbon atom for the (100) face (~18%) and two carbon atoms for the (001) face (~23%). Notably, nitrogen atoms participated less frequently in both facets. These interaction patterns highlight the role of PVP's carbonyl and methylene groups in stabilizing adsorption to the stacking interface, consistent with our experimental observation that carbonyl-containing polymers selectively inhibit growth along the (100) face. Without re-optimization, we used the snapshots of the closest PVP monomer and guanine molecule from the unbiased trajectories to determine their interaction energy with density functional theory (DFT) as implemented

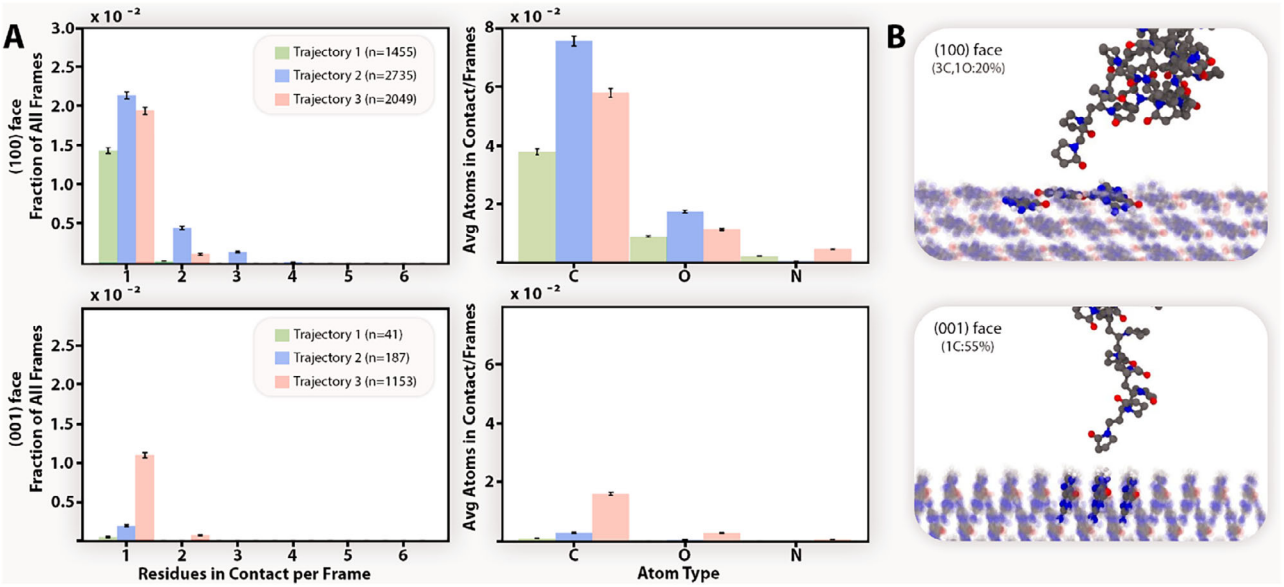

FIGURE 6 | Mapping PVP–guanine close contacts at the (100) and (001) faces. (A) Left column: Fraction of simulation frames in which a given number of PVP residues were within 5 Å of the guanine surface, for the (100) face (top) and (001) face (bottom). Each colored bar represents the frequency with which a specific number of residues were simultaneously in contact with the surface, with color distinguishing among the three independent 1 μs trajectories per interface. Note: *n* indicates the total number of contact frames per trajectory (out of 100,000), and error bars show standard errors estimated from bootstrapping. Right Column: Average number of polymer heavy-atom contacts per frame for each atom type (C, O, N), shown for the (100) face (top) and (001) face (bottom). Error bars represent standard errors estimated from bootstrapping. B) Representative snapshots from unbiased MD trajectories showing the most frequent heavy-atom contact motifs at the (100) face (top) and the (001) face (bottom). For the (100) face, PVP predominantly contacts the surface via two methylene carbons and one carbonyl oxygen; on the (001) face, single-carbon contacts predominate. Gray: Carbon, blue: Nitrogen, and red: Oxygen.

in Orca 6.1.0 [73, 74]. For these calculations, we employed the ωB97X-D [75] functional along with an implicit solvent treatment for formamide using the conductor-like polarizable continuum model (CPCM) [76] (see the Supporting Information for full computational details). These calculations revealed that PVP monomers interact most strongly with guanine at the (100) face (−7.34 kJ/mol) compared to the (001) face (−2.05 kJ/mol), in good agreement with our umbrella sampling results (Figure S17). To investigate the origin of this enhanced interaction, we analyzed the correlation between interaction energy and the distance from the guanine heavy-atom center of mass to either the carbonyl carbon or oxygen of PVP (Figure S18). The position of the carbonyl carbon showed a larger Pearson correlation coefficient with the interaction energy (r = 0.75) than the carbonyl oxygen (r = 0.58), indicating that it is the more critical contributor to the favorable interactions upon complexation with the (100) face. Further analysis revealed that the strongest interactions occur when the carbonyl bond adopts a flat orientation relative to the guanine surface, allowing close contact between the carbonyl carbon and the π-system (Figure S19). These findings support the hypothesis that the partial positive carbonyl carbon is primarily responsible for the favorable interaction at the (100) face.

3 | Discussion

Our results demonstrate that polymers can exert exquisite control over the morphology of guanine crystals, not only replicating the features of biogenic crystals, but also expanding them by providing access to new crystal morphologies. By systematically varying the polymer's composition, we identified several key factors that govern its influence on crystal morphology. First and foremost, the polymer must be able to engage in multi-point interactions with the crystal surface. The failure of polyethylene or of small molecule modifiers to produce a strong effect highlights that a single-point adsorption is not sufficient; the polymer's backbone provides a scaffold for cooperative binding. This likely means that multiple functional groups on one polymer chain can attach simultaneously across a crystalline domain, increasing the residence time and coverage on that facet. In essence, the polymer acts as a flexible "cover" that blankets a particular crystal face. If the cover is incomplete or keeps detaching, as would be the case for a small molecule that binds and unbinds rapidly, leaving the crystal face free to grow. Thus, one design principle is that multivalency matters: effective morphology modifiers for molecular crystals should present arrays of interacting groups: polymers, oligomers, or perhaps self-assembling supramolecular modifiers, rather than just individual molecules.

In addition to multivalency, steric effects play a crucial role in determining how efficiently a polymer can pack and interact with the crystal surface. Our systematic variation of side-chain length showed that increasing steric bulk weakens the polymer's ability to inhibit growth along the stacking direction, leading to progressively thicker crystals. This suggests that optimal surface binding requires a balance, functional groups that are sufficiently compact to pack densely on the (100) surface, yet large enough

to provide stable adsorption through dispersion and dipolar interactions.

Our analysis further indicates that polymer chain length have only a limited influence on crystal morphology under the conditions studied. Across two orders of magnitude in molecular weight, guanine crystals exhibited broadly similar aspect ratios, with only minor variations that did not show a clear or systematic trend. These observations suggest that, once a sufficient chain length is reached to enable multivalent surface binding, further increases in molecular weight have little additional effect on habit. Thus, while chain length may subtly modulate the kinetics of crystal growth, the dominant control over crystal shape arises from surface chemistry and facet-specific adsorption rather than from chain-length– or viscosity-dependent effects.

Second, the chemical identity of the functional groups on the modifier is critical. Comparing different polymers reveals a range of effects that can be correlated with how those functional groups interact with guanine's crystal surfaces. The most effective modifiers in producing plate-like morphology: PVP, PVA, and PVP-co-VA, all share a common functionality, the carbonyl group, which we found to be essential for engaging the π-stacking interface. A carbonyl provides a dipole that can align with the guanine π-cloud, akin to how certain aromatic modifiers or cations can π-stack or electrostatically stick to flat aromatic surfaces [66]. This is reminiscent of strategies in colloidal chemistry to stabilize layered materials: for example, graphene sheets (similarly planar and π-rich) can be exfoliated and stabilized in solution by polymers like PVP or by pyrene-based surfactants that bind via π–π interactions [62, 63]. In guanine's case, the carbonyl-bearing polymer likely inserts between or atop guanine layers, "capping" the hydrophobic face and preventing further layer addition, similarly to how some biogenic macromolecules are hypothesized to cap the (100) face in vivo [25]. This mechanism is supported by quantum chemical calculations based on geometries extracted from the unbiased molecular dynamics simulations of PVP interacting with the (100) and (001) faces of guanine (Supporting Information for full computational details). Consistent with our umbrella sampling results, these DFT calculations revealed that PVP monomers interact more strongly with the (100) face than with the (001) face. Further analysis showed that the strongest interactions occur when the partial positive carbonyl carbon is positioned close to guanine's π-system and the carbonyl bond lies flat relative to the guanine molecular plane. In contrast, the proximity of the carbonyl oxygen to the guanine surface was a less reliable predictor of interaction strength, supporting the key role of the carbonyl carbon in the favorable interactions in the (100) face.

When the polymer's functional group lacks a strong dipole this capping cannot occur, hence normal growth resumes. The carbonyl groups tip the balance by slowing down the growth in the stacking direction, thereby favoring 2D growth, as thin plates, over the formation of 3D prisms.

Third, we observed that the polarity and hydrogen bonding ability of the functional groups have a strong impact on the polymer-crystal interactions. Moderately polar groups like esters and lactams are effective at targeting the nonpolar crystal face without excessively disrupting other interactions. If the groups are more polar (—COOH, —$CONH_2$), the polymer's binding preferences seem to broaden or shift, resulting in loss of the specific inhibition of the *a*-axis growth. In those cases, the modifiers may bind strongly to edge sites, leading to almost 1D growth, in strong contrast to the plate-like crystals observed for PVP and PVA. Thus, expanding the range of morphologies achieved for anhydrous guanine crystals, with, for example, slender needles elongated along the *a*-axis, which were previously only observed for guanine monohydrate. This ability to fine-tune crystal morphology could have implications for optimizing optical, mechanical, and electronic properties.

In vivo, guanine crystals form intracellularly within a membrane-bound organelle [77]. The macromolecular fibers identified in these cells are believed to provide a hydrophobic, periodic surface that encourages guanine molecules to first organize into ordered hydrogen bond layers. These fibers may present i) a repetitive array of binding sites that provide multivalency, ii) a nonpolar surface that can facilitate the facet-selective affinity for the hydrophobic face of guanine, and iii) perhaps specific functional groups, e.g., certain amino acid side chains, that interact optimally with guanine. These qualities could be parallel to what we found to be important in our polymer modifiers.

The fact that PVP can mimic the biogenic fiber's role suggests that the core requirements are more physical-chemical (hydrophobic/π/π interactions, dipolar capping) than biological per se. Nature's solution was a macromolecular scaffold, while we and others used a synthetic polymer [55, 56], yet both converge to restrict guanine's growth in the *a*-direction. In biological systems, guanine crystallization occurs on macromolecular fibres that are typically ~20 nm in diameter and organized into bundles within membrane-bound organelles, providing a nanoscale framework for nucleation and subsequent crystal growth [25]. In contrast, the polymers used in our experiments, such as 40 kDa PVP, have a radius of gyration of approximately 6–9 nm [78], comparable in scale but lacking the rigid fibrillar architecture and periodic organization of the natural scaffolds. This similarity in length scale may allow the polymers to mimic some aspects of the molecular environment, such as multivalent binding and transient surface adsorption, yet they do not replicate the directional, preorganized templating provided by biological fibres. It is also important to note that guanine crystals in both systems begin as nanoscale nuclei that grow into much larger plates during maturation. In our experiments, the polymers most likely interact dynamically with the crystal surfaces throughout this growth process. Thus, while both systems operate on similar nanoscale dimensions, templating in our in vitro system arises from dynamic surface interactions rather than the structural confinement and molecular guidance characteristic of natural scaffolds.

In contrast to the highly regulated biological environment, where guanine crystallization occurs within confined, membrane-bound organelles (iridosomes) [79], our experiments were performed in bulk solution without spatial confinement or preassembled macromolecular scaffolds. In vivo, crystallization

is orchestrated by an integrated network of fibers, regulatory proteins, and small molecules that act cooperatively to direct nucleation and growth. Under our in vitro conditions, by contrast, the polymers and small molecules act independently in a more stochastic setting. Furthermore, the roles of small molecules differ between the two systems: in biogenic crystals, metabolites such as hypoxanthine are incorporated into the crystal lattice as dopants that subtly modulate internal structure and stability, whereas in our system they remain in solution and interact transiently with the crystal surface.

Despite the differences, the convergence of solutions, hints at a unifying principle: to obtain a thin, plate-like morphology of a layered crystal, one must selectively impede layer stacking while promoting 2D growth. Organisms likely achieve this with pre-assembled scaffolds and selective capping proteins, leading to multiple thin crystal leaflets that merge. In our case, a polymer in solution likely adsorbs to nascent crystal nuclei and fulfills a similar role of capping the top layer, yielding a single crystal that expands laterally.

In nature, organisms harness molecular crystals for a wide variety of optical phenomena by adopting diverse hierarchical structures [10, 11]. For instance, ultra-thin platelets can form spherical assemblages in certain shrimp, producing brilliant whiteness [80]. In some crustaceans, dynamic arrangements of guanine crystals function as tunable reflectors that can switch the organism from transparent to reflective, aiding camouflage and communication [30, 31]. These examples rely on precise control over crystal size, shape, and orientation. They highlight that by modulating crystal growth, a wide range of photonic properties can be achieved. From a materials science perspective, this is a powerful inspiration: if we can learn to control molecular crystal morphology and assembly as deftly as nature, we could fabricate new optical materials that are biocompatible and lightweight. In that sense, guanine is especially attractive given its high refractive index and ability to form multiple polymorphs and nanostructures.

Finally, this study contributes to the understanding of organic crystallization mechanisms. Guanine crystallization has emerged as a model for nonclassical nucleation and assembly processes [25, 43], and our results add the dimension of how an external modifier influences those pathways. The absence of any new crystalline order or major lattice distortion in our experiments suggests that the polymer influences the growth kinetics, rather than being incorporated. This kind of guidance is common in biomineralization but challenging to mimic in synthetic systems. By showing success in the case of guanine, we pave the way for applying similar tactics to other crystals where morphology is critical, e.g., pharmaceuticals, organic semiconductors, and pigments.

In summary, controlling crystal morphology by design is becoming an achievable goal, also thanks to insights from biological systems. Our work bridges biomineralization and materials chemistry, demonstrating that by harnessing polymer-crystal interactions, we can not only gain new insights on how organisms achieve their crystal architectures, but also translate that understanding into predictive design rules for novel materials. Moving forward, integrating biomimetic strategies with advanced computational modeling and high-throughput experimentation could rapidly expand our ability to form crystals with tailor-made morphologies and functions. This approach could also benefit from utilizing more natural modifiers, such as amino acid-based peptides that could be engineered to have a specific structure, periodicity, and chemistry. This convergence of fields opens new avenues to create optical and functional materials inspired by, and potentially even surpassing, nature's own crystalline masterpieces.

Acknowledgements

This work was supported by an ERC Starting (Grants Nos.: 101077470, "CRYSTALCELL") and by the Israel Science Foundation (Grants No.: 691/22) awarded to D.G. The authors thank Prof. Lia Addadi for her advice and helpful discussions on this project. The authors thank Dr. Neta Varsano for her contribution to figure design and Ms. Rachael Deis for her contribution to zebrafish crystals isolation. B.H. acknowledges support from the Israel Science Foundation (Grants Nos.: 1037/22 and 1312/22) and the Pazy Foundation of the IAEC-UPBC (Grants No.: 415–2023).

Conflicts of Interest

The authors declare no conflicts of interest.

Data Availability Statement

The data that support the findings of this study are available in the supplementary material of this article.

References

1. J. H. Moon and S. Yang, "Chemical Aspects of Three-Dimensional Photonic Crystals," *Chemical Reviews* 110 (2010): 547–574, https://doi.org/10.1021/cr900080v.

2. W. S. Yang, L. Jiao, W. Liu, Y. L. Deng, and H. Q. Dai, "Morphology Control for Tunable Optical Properties of Cellulose Nanofibrils Films," *Cellulose* 25 (2018): 5909–5918, https://doi.org/10.1007/s10570-018-1974-1.

3. C. Sui, Y. S. Zhao, Z. S. Zhang, et al., "Morphology-Controlled Tensile Mechanical Characteristics in Graphene Allotropes," *ACS Omega* 2 (2017): 3977–3988.

4. J. Bisquert, "Effects of Morphology on the Functionality of Organic Electronic Devices," *The Journal of Physical Chemistry Letters* 3 (2012): 1515–1516, https://doi.org/10.1021/jz300600j.

5. Y. Diao, L. Shaw, Z. A. Bao, and S. C. B. Mannsfeld, "Morphology Control Strategies for Solution-processed Organic Semiconductor Thin Films," *Energy Environ Science* 7 (2014): 2145–2159, https://doi.org/10.1039/C4EE00688G.

6. W. M. Awad, D. W. Davies, D. Kitagawa, et al., "Mechanical Properties and Peculiarities of Molecular Crystals," *Chemical Society Reviews* 52 (2023): 3098–3169, https://doi.org/10.1039/D2CS00481J.

7. A. G. Shtukenberg, M. D. Ward, and B. Kahr, "Crystal Growth With Macromolecular Additives," *Chemical Reviews* 117 (2017): 14042–14090, https://doi.org/10.1021/acs.chemrev.7b00285.

8. Y. Barzilay, Z. Eyal, Y. Noy, et al., "Specialized Molecular Pathways Drive the Formation of Light- scattering Assemblies in Leucophores " *Proceedings of the National Academy of Sciences* 122 (2025): 2424979122.

9. M. F. Land, "The Physics and Biology of Animal Reflectors," *Progress in Biophysics and Molecular Biology* 24 (1972): 75–106, https://doi.org/10.1016/0079-6107(72)90004-1.

10. D. Gur, B. A. Palmer, S. Weiner, and L. Addadi, "Light Manipulation by Guanine Crystals in Organisms: Biogenic Scatterers, Mirrors, Multilayer

Reflectors and Photonic Crystals," *Advanced Functional Materials* 27 (2017): 1603514.

11. B. A. Palmer, D. Gur, S. Weiner, L. Addadi, and D. Oron, "The Organic Crystalline Materials of Vision: Structure-Function Considerations from the Nanometer to the Millimeter Scale," *Advanced Materials* 30 (2018): 1800006.

12. S. Weiner and L. Addadi, "Crystallization Pathways in Biomineralization," *Annual Review of Materials Research* 41 (2011): 21–40.

13. R. Seidel, K. Handrich, M. Albéric, et al., "Comparative Structural Analysis of Stereom Polymorphs in the Sea Urchin Test," *Faraday Discussions* 261 (2025): 340–358, https://doi.org/10.1039/D5FD00033E.

14. Y. Politi, L. Bertinetti, P. Fratzl, and F. G. Barth, "The spider cuticle: a remarkable material toolbox for functional diversity," *Philosophical Transactions of the Royal Society A* 379 (2021): 2206.

15. J. L. Drake, Y. Benayahu, I. Polishchuk, B. Pokroy, I. Pinkas, and T. Mass, "Sclerites of the soft coral Ovabunda macrospiculata (Xeniidae) are predominantly the metastable CaCO3 polymorph vaterite," *Acta Biomaterialia* 135 (2021): 663–670, https://doi.org/10.1016/j.actbio.2021.08.051.

16. Z. A. Jia, M. C. Fernandes, Z. F. Deng, et al., "Microstructural design for mechanical-optical multifunctionality in the exoskeleton of the flower beetle Torynorrhina flammea," *Proceedings of the National Academy of Sciences of the United States of America* 118, no. 25 (2021).

17. Z. Eyal, L. Krounbi, O. Ben Joseph, et al., "The Variability in the Structural and Functional Properties of Coccolith Base Plates," *Acta Biomaterialia* 148 (2022): 336–344, https://doi.org/10.1016/j.actbio.2022.06.027.

18. C. A. Schmidt, E. Tambutté, A. A. Venn, et al., "Myriad Mapping of nanoscale minerals reveals calcium carbonate hemihydrate in forming nacre and coral biominerals," *Nature Communications* 15, no. 1 (2024).

19. M. Kolle, P. M. Salgard-Cunha, M. R. J. Scherer, et al., "Mimicking the colourful wing scale structure of the Papilio blumei butterfly," *Nature Nanotechnol* 5, no. 7 (2010): 511–515, https://doi.org/10.1038/nnano.2010.101.

20. R. Lemanis and I. Zlotnikov, "Finite Element Analysis as a Method to Study Molluscan Shell Mechanics," *Advanced Engineering Materials* 20, no. 3 (2018), https://doi.org/10.1002/adem.201700939.

21. J. Aizenberg, A. Tkachenko, S. Weiner, L. Addadi, and G. Hendler, "Calcitic microlenses as part of the photoreceptor system in brittlestars," *Nature* 412, no. 6849 (2001): 819–822, https://doi.org/10.1038/35090573.

22. J. Aizenberg, G. Lambert, S. Weiner, and L. Addadi, "Factors Involved in the Formation of Amorphous and Crystalline Calcium Carbonate: A Study of an Ascidian Skeleton," *Journal of the American Chemical Society* 124, no. 1 (2002): 32–39, https://doi.org/10.1021/ja016990l.

23. A. Levy-Lior, B. Pokroy, B. Levavi-Sivan, L. Leiserowitz, S. Weiner, and L. Addadi, "Biogenic Guanine Crystals from the Skin of Fish May Be Designed to Enhance Light Reflectance," *Crystal Growth & Design* 8, no. 2 (2008): 507–511, https://doi.org/10.1021/cg0704753.

24. D. Gur, M. Pierantoni, N. E. Dov, et al., "Guanine Crystallization in Aqueous Solutions Enables Control over Crystal Size and Polymorphism," *Crystal Growth & Design* 16, no. 9 (2016): 4975–4980, https://doi.org/10.1021/acs.cgd.6b00566.

25. Z. Eyal, R. Deis, N. Varsano, et al., "Plate-like Guanine Biocrystals Form via Templated Nucleation of Crystal Leaflets on Preassembled Scaffolds," *Journal of the American Chemical Society* 144, 49 (2022): 22440–22445, https://doi.org/10.1021/jacs.2c11136.

26. A. Wagner, A. Upcher, R. Maria, et al., "Macromolecular sheets direct the morphology and orientation of plate-like biogenic guanine crystals," *Nature Communications* 14, no. 1 (2023), https://doi.org/10.1038/s41467-023-35894-6.

27. K. Hinrichs, S. D. Silaghi, C. Cobet, N. Esser, and D. R. T. Zahn, "Ellipsometry From Infrared to Vacuum Ultraviolet: Structural Properties of Thin Anisotropic Guanine Films on Silicon," *Physica Status Solidi (b)* 242 (2005): 2681–2687, https://doi.org/10.1002/pssb.200541154.

28. S. Kinoshita, S. Yoshioka, and J. Miyazaki, "Physics of structural colors," *Reports on Progress in Physics* 71, no. 7 2008.

29. L. M. Beck, V. J. Yallapragada, A. Upcher, B. A. Palmer, L. Addadi, and D. Oron, "Measuring the optical properties of nanoscale biogenic spherulites," *Optics Express* 29, no. 13 (2021): 20863–20871, https://doi.org/10.1364/OE.430376.

30. D. Gur, B. Leshem, M. Pierantoni, et al., "Structural Basis for the Brilliant Colors of the Sapphirinid Copepods," *Journal of the American Chemical Society* 137, no. 26 (2015): 8408–8411, https://doi.org/10.1021/jacs.5b05289.

31. D. Gur, B. Leshem, V. Farstey, D. Oron, L. Addadi, and S. Weiner, "Light-Induced Color Change in the Sapphirinid Copepods: Tunable Photonic Crystals," *Advanced Functional Materials* 26 (2015): 1393–1399, https://doi.org/10.1002/adfm.201504339.

32. B. A. Palmer, G. J. Taylor, V. Brumfeld, et al., "The image-forming mirror in the eye of the scallop," *Science* 358 (2016): 1172–1175, https://doi.org/10.1126/science.aam9506.

33. D. M. Guo, Y. Q. Liu, X. B. Hou, et al., "Formation Mechanism of Twinned β-form Anhydrous Guanine Platelets in Scallop Eyes," *CrystEngComm* 25 (2023): 4521–4530, https://doi.org/10.1039/D3CE00485F.

34. D. Gur, J. D. Nicolas, V. Brumfeld, O. Bar-Elli, D. Oron, and G. Levkowitz, "The Dual Functional Reflecting Iris of the Zebrafish," *Advancement of Science* 5 (2018): 1800338.

35. L. Addadi, L. Kronik, L. Leiserowitz, D. Oron, and S. Weiner, "Organic Crystals and Optical Functions in Biology: Knowns and Unknowns," *Advanced Materials* 36, no. 38 (2024).

36. A. Hirsch, D. Gur, I. Polishchuk, et al., ""Guanigma": The Revised Structure of Biogenic Anhydrous Guanine," *Chemistry of Materials* 27 (2024): 8289–8297.

37. K. Guille and W. Clegg, "Anhydrous guanine: A synchrotron study," *Acta Crystallographica Section C Crystal Structure Communications* 62 (2015): o515–o517, https://doi.org/10.1107/S0108270106026011.

38. A. Jantschke, I. Pinkas, A. Hirsch, et al., "Anhydrous β-guanine crystals in a marine dinoflagellate: Structure and suggested function," *Journal of Structural Biology* 207 (2006): 12–20, https://doi.org/10.1016/j.jsb.2019.04.009.

39. A. Hirsch, B. A. Palmer, N. Elad, et al., "Biologically Controlled Morphology and Twinning in Guanine Crystals," *Angewandte Chemie, International Edition* 56, no. 32 (2017): 9420–9424.

40. Y. Tsarfati, I. Biran, E. Wiedenbeck, L. Houben, H. Cölfen, and B. Rybtchinski, "Continuum Crystallization Model Derived from Pharmaceutical Crystallization Mechanisms," *ACS Central Science* 7, no. 5 (2021): 900–908, https://doi.org/10.1021/acscentsci.1c00254.

41. D. Gur, Y. Politi, B. Sivan, P. Fratzl, S. Weiner, and L. Addadi, "Guanine-Based Photonic Crystals in Fish Scales Form From an Amorphous Precursor," *Angewandte Chemie International Edition* 52 (2013): 388–391, https://doi.org/10.1002/anie.201205336.

42. A. Wagner, V. Ezersky, R. Maria, et al., "The Non-Classical Crystallization Mechanism of a Composite Biogenic Guanine Crystal," *Advanced Materials* 34 (2022): 2202242.

43. S. S. Indri, F. M. Dietrich, A. Wagner, et al., "Guanine Crystallization by Particle Attachment," *Journal of the American Chemical Society* 147 (2025): 19139–19147, https://doi.org/10.1021/jacs.5c04543.

44. N. Pinsk, A. Wagner, L. Cohen, et al., "Biogenic Guanine Crystals Are Solid Solutions of Guanine and Other Purine Metabolites," *Journal of the American Chemical Society* 144 (2022): 5180–5189, https://doi.org/10.1021/jacs.2c00724.

45. J. D. Taylor, "The Effects of Intermedin on the Ultrastructure of Amphibian Iridophores," *General and Comparative*

Endocrinology 12 (1969): 405–416, https://doi.org/10.1016/0016-6480(69)90157-9.

46. R. Deis, T. Lerer-Goldshtein, O. Baiko, et al., "Genetic Control Over Biogenic Crystal Morphogenesis in Zebrafish," *Nature Chemical Biology* 21 (2025): 383–392, https://doi.org/10.1038/s41589-024-01722-1.

47. A. Wagner, A. Hill, T. Lemcoff, et al., "Rationalizing the Influence of Small-Molecule Dopants on Guanine Crystal Morphology," *Chem Mater* 36 (2024): 8910–8919.

48. B. T. Roy, L. J. Hasselt, R. Young, et al., "Guanine Crystal Formation at Physiological pH," *Crystal Growth & Design* 25, no. 12 (2025): 4316–4324.

49. C. R. Li, N. K. Wittig, T. E. K. Christensen, et al., "Confinement-Controlled Crystallization of Guanine," *Chemistry of Materials* 36 (2024): 6038–6046, https://doi.org/10.1021/acs.chemmater.4c00550.

50. N. K. Wittig, T. E. K. Christensen, T. A. Grünewald, and H. Birkedal, "Vase-Like β-Polymorph Guanine Crystal Aggregates Formed at the Air–Water Interface," *ACS Materials Letters* 2 (2020): 446–452, https://doi.org/10.1021/acsmaterialslett.9b00447.

51. L. Alus, L. Houben, N. Shaked, et al., "Bio-Inspired Crystalline Core-Shell Guanine Spherulites," *Advanced Materials* 36 (2024).

52. Y. R. Ma, F. H. Chen, Y. R. Hu, Y. N. Liu, and L. M. Qi, "Controlled Crystallization of Twinned Crystalline Guanine Microplatelets," *CrystEngComm* 21 (2019): 6346–6353, https://doi.org/10.1039/C9CE00920E.

53. B. B. Wu, Y. N. Liu, F. H. Chen, et al., "Investigation on the Formation Mechanism of Twinned Crystals of Hypoxanthine-doped Beta-phase Anhydrous Guanine Microplatelets," *CrystEngComm* 23 (2021): 3444–3452, https://doi.org/10.1039/D1CE00148E.

54. F. H. Chen, Y. R. Ma, and L. M. Qi, "Synthesis of Porous Microplatelets of α Form Anhydrous Guanine in DMSO/Water Mixed Solvents," *CrystEngComm* 24 (2022): 4215–4223, https://doi.org/10.1039/D1CE01709H.

55. Y. Oaki, S. Kaneko, and H. Imai, "Morphology and Orientation Control of Guanine Crystals: A Biogenic Architecture and Its Structure Mimetics," *Journal of Materials Chemistry* 22 (2012): 22686, https://doi.org/10.1039/c2jm33047d.

56. F. H. Chen, Y. N. Liu, L. Li, L. M. Qi, and Y. R. Ma, "Synthesis of Bio-Inspired Guanine Microplatelets: Morphological and Crystallographic Control," *Chemistry – A European Journal* 26 (2020): 16228–16235, https://doi.org/10.1002/chem.202003156.

57. L. M. Salonen, M. Ellermann, and F. Diederich, "Aromatic Rings in Chemical and Biological Recognition: Energetics and Structures," *Angewandte Chemie International Edition* 50 (2011): 4808–4842, https://doi.org/10.1002/anie.201007560.

58. M. H. Al Mughram, C. Catalano, J. P. Bowry, M. K. Safo, J. N. Scarsdale, and G. E. Kellogg, "3D Interaction Homology: Hydropathic Analyses of the "π–Cation" and "π–π" Interaction Motifs in Phenylalanine, Tyrosine, and Tryptophan Residues," *Journal of Chemical Information and Modeling* 61 (2021): 2937–2956, https://doi.org/10.1021/acs.jcim.1c00235.

59. A. Thomas, R. Meurisse, B. Charloteaux, and R. Brasseur, "Aromatic side-chain interactions in proteins. I. Main structural features," *Proteins: Structure, Function, and Bioinformatics* 48 (2002): 628–634, https://doi.org/10.1002/prot.10190.

60. R. Calinsky and Y. Levy, "Aromatic Residues in Proteins: Re-Evaluating the Geometry and Energetics of π–π, Cation–π, and CH–π Interactions," *The Journal of Physical Chemistry B* 128 (2024): 8687–8700, https://doi.org/10.1021/acs.jpcb.4c04774.

61. J. Wang and L. S. Yao, "Dissecting C-H•••π and N-H•••π Interactions in Two Proteins Using a Combined Experimental and Computational Approach," *Scientific Reports* 9 (2019): 20149.

62. D. Parviz, S. Das, H. S. T. Ahmed, F. Irin, S. Bhattacharia, and M. J. Green, "Dispersions of Non-Covalently Functionalized Graphene With Minimal Stabilizer," *ACS Nano* 6 (2012): 8857–8867, https://doi.org/10.1021/nn302784m.

63. A. B. Bourlinos, V. Georgakilas, R. Zboril, T. A. Steriotis, A. K. Stubos, and C. Trapalis, "Aqueous-phase Exfoliation of Graphite in the Presence of Polyvinylpyrrolidone for the Production of Water-soluble Graphenes," *Solid State Communications* 149 (2009): 2172–2176, https://doi.org/10.1016/j.ssc.2009.09.018.

64. M. K. Cyrański, M. Gilski, M. Jaskólski, and T. M. Krygowski, "On the Aromatic Character of the Heterocyclic Bases of DNA and RNA," *The Journal of Organic Chemistry* 68 (2003): 8607–8613.

65. O. A. Stasyuk, H. Szatylowicz, and T. M. Krygowski, "Aromaticity of H-bonded and Metal Complexes of Guanine Tautomers," *Structural Chemistry* 27 (2016): 111–118, https://doi.org/10.1007/s11224-015-0605-9.

66. P. Li, E. C. Vik, J. M. Maier, et al., "Electrostatically Driven CO–π Aromatic Interactions," *Journal of the American Chemical Society* 141 (2019): 12513–12517, https://doi.org/10.1021/jacs.9b06363.

67. C. W. Yin, H. B. Ye, Y. Hai, H. X. Zou, and L. You, "Aromatic-Carbonyl Interactions as an Emerging Type of Non-Covalent Interactions," *Advancement of Science* 11 (2024): 2310337.

68. J. E. Leffler and E. Grunwald, *Rates and Equilibria of Organic Reactions as Treated by Statistical, Thermodynamic, and Extrathermodynamic Methods*, (Wiley, 1963).

69. B. R. Brooks, R. E. Bruccoleri, B. D. Olafson, D. J. States, S. Swaminathan, and M. Karplus, "CHARMM:A program for macromolecular energy, minimization, and dynamics calculations," *Journal of Computational Chemistry* 4 (1983): 187–217, https://doi.org/10.1002/jcc.540040211.

70. K. Vanommeslaeghe, E. Hatcher, C. Acharya, et al., "CHARMM general force field: A force field for drug-like molecules compatible with the CHARMM all-atom additive biological force fields," *Journal of Computational Chemistry* 31 (2010): 671–690.

71. D. Van der Spoel, E. Lindahl, B. Hess, G. Groenhof, A. E. Mark, and H. J. C. Berendsen, "GROMACS: Fast, Flexible, and Free," *Journal of Computational Chemistry* 26 (2005): 1701–1718, https://doi.org/10.1002/jcc.20291.

72. A. Lindahl and V. Hess & der Spoel, GROMACS 20196 Source Code (2020), Zenodo, https://doi.org/10.5281/zenodo.3685922.

73. F. Neese, "Software Update: The ORCA Program System—version 6.0," *Wiley Interdisciplinary Reviews: Computational Molecular Science* 15 (2025): 70019.

74. F. Neese, "The SHARK Integral Generation and Digestion System," *Journal of Computational Chemistry* 44 (2023): 381–396, https://doi.org/10.1002/jcc.26942.

75. J. Chai and M. Head-Gordon, "Long-range corrected hybrid density functionals with damped atom–atom dispersion corrections," *Physical Chemistry Chemical Physics* 10 (2008): 6615, https://doi.org/10.1039/b810189b.

76. M. Garcia-Ratés and F. Neese, "Effect of the Solute Cavity on the Solvation Energy and Its Derivatives Within the Framework of the Gaussian Charge Scheme," *Journal of Computational Chemistry* 41 (2020): 922–939, https://doi.org/10.1002/jcc.26139.

77. A. Levy-Lior, E. Shimoni, O. Schwartz, et al., "Guanine-Based Biogenic Photonic-Crystal Arrays in Fish and Spiders," *Advanced Functional Materials* 20 (2010): 320–329, https://doi.org/10.1002/adfm.200901437.

78. L. Sapir, C. B. Stanley, and D. Harries, "Properties of Polyvinylpyrrolidone in a Deep Eutectic Solvent," *The Journal of Physical Chemistry A* 120 (2016): 3253–3259, https://doi.org/10.1021/acs.jpca.5b11927.

79. Z. Eyal, R. Deis, A. Gorelick-Ashkenazi, et al., "pH Variations Enable Guanine Crystal Formation Within Iridosomes," *Nature Chemical Biology* 22 (2026): 19–27, https://doi.org/10.1038/s41589-025-02020-0.

80. T. Lemcoff, L. Alus, J. S. Haataja, et al., "Brilliant Whiteness in Shrimp From Ultra-thin Layers of Birefringent Nanospheres," *Nature Photonics* 17 (2023): 485–493, https://doi.org/10.1038/s41566-023-01182-4.

Supporting Information

Additional supporting information can be found online in the Supporting Information section.

Supporting File: smll72227-sup-0001-SuppMat.pdf